THE HEAO-3 COSMIC RAY ISOTOPE SPECTROMETER†

M. BOUFFARD, J. J. ENGELMANN, L. KOCH, and A. SOUTOUL
Centre d'Etudes Nucleaires de Saclay, Gif-sur-Yvette, France

and

N. LUND, B. PETERS, and I. L. RASMUSSEN
Danish Space Research Institute, Lyngby, Denmark

(*Representing the Saclay-Copenhagen Collaboration**)

(Received 27 March, 1981)

Abstract. This paper describes the Cosmic Ray Isotope instrument launched aboard the HEAO-3 satellite on September 20, 1979. The primary purpose of the experiment is to measure the isotopic composition of cosmic ray nuclei from Be-7 to Fe–58 over the energy range 0.5 to 7 GeV/nucleon. In addition charge spectra will be measured between beryllium and tin over the energy range 0.5 to 25 GeV/nucleon. The charge and isotope abundances measured by the experiment provide essential information needed to further our understanding of the origin and propagation of high energy cosmic rays. The instrument consists of 5 Cerenkov counters, a 4 element neon flash tube hodoscope and a time-of-flight system. The determination of charge and energy for each particle is based on the multiple Cerenkov technique and the mass determination will be based upon a statistical analysis of particle trajectories in the geomagnetic field.

1. Introduction

The determination of the charge and mass composition of the primary cosmic radiation is important for many astrophysical problems, in particular stellar nucleosynthesis and high energy particle acceleration mechanisms. It will allow the question about the existence of a galactic cosmic ray halo to be addressed, thereby giving information about the strength and topology of the galactic

† Originally submitted to the journal *Space Science Instrumentation.*

* The Saclay-Copenhagen Collaboration consists of the authors and the following members:

Scientific support and data processing:
B. Byrnak[2], M. Cantin[1], F. Gaulier[1], P. Goret[1], H. Jakobsen[2], J. Jorrand[1], P. Masse[1], N. Petrou[1], M. Rotenberg[2], and N. J. Westergaard[2].

Engineering and testing:
R. Chaufriasse[3], R. Comte[1], J. Cretolle[1], R. Duc[1], O. Funch[2], J. Giraudbit[3], B. Jacquemin[1], P. Jonasson[2], P. Keirle[1], A. Kjaer[2], A. Lavaitte[1], M. Lesueur[1], Y. Maubras[1], J. Maudhuit[1], P. Mestrau[1], J. Midan[3], P. Mogensen[2], K. Omoe[2], M. Pernod[1], M. Petersson[2], Y. Rio[1], A. Robin[1], J. Rollin[1], A. Roy[1], and J. Verdun[1].

[1] *Centre d'Etudes Nucleaires de Saclay, B.P.2, 91190 Gif-sur-Yvette, France.*
[2] *Danish Space Research Institute, Lundtoftevej 7, DK–2800 Lyngby, Denmark.*
[3] *Centre National d'Etudes Spatiales, Toulouse, France.*

Astrophysics and Space Science **84** (1982) 3–33. 0004–640X/82/0841–0003$04.65.

magnetic field. This information can best be obtained at relativistic energies, where composition changes due to solar modulation and ionization losses are negligible and where nuclear interaction cross-sections are constant or vary only slowly with energy.

However, at the high energies where the results are simpler to interpret, the measurements are more difficult to perform. Especially the determination of the mass becomes complicated, as the dE/dX-total E methods which are useful at lower energies, fail at multi-GeV energies, where the particle range is an order of magnitude greater than the mean nuclear interaction length. At present the only possibility to obtain a mass estimate is to measure the magnetic rigidity

$$R = P\frac{M}{Z}, \tag{1}$$

where M is the atomic mass, P the particle momentum/nucleon and Z is the charge. As no superconducting magnet of sufficient strength, size and cryostat lifetime which can separate isotopes in this energy range is as yet available, we have developed a method based upon the use of the geomagnetic field. Figure 1 compares the charge and energy range of the present experiment with the ranges of previous experiments.

By comparing fluxes of particles with accurately measured charge and momentum obtained at different geomagnetic cut-off conditions, one can in a conceptually straightforward manner determine the mean mass of the particles in each element [1–3]. By a more detailed analysis based upon distinct features of the cut-off we hope to determine the individual masses of a smaller sample of particles [4, 5].

The measurement accuracy required for isotope determinations has led us to design an instrument using Cerenkov counters only. This ensures good charge resolution at high charges, as Cerenkov counters in contrast to scintillation counters do not saturate, even for very high ionization densities. In order to obtain precise momentum determinations over an extended range it has been necessary to use a sequence of 5 counters and to develop new radiator materials with low refractive indices.

The precision needed also demanded the use of thick radiators, i.e., many $g\,cm^{-2}$ in the particle path. The resulting high interaction rate means that the instrument is more suited to detailed comparisons between neighbouring elements than to the determination of absolute abundances.

2. Scientific Objectives

The HEAO-3 C2 instrument is designed to determine:

- The mass composition of the most abundant elements between beryllium and iron in the energy range 0.5 to 7 GeV/nucleon;

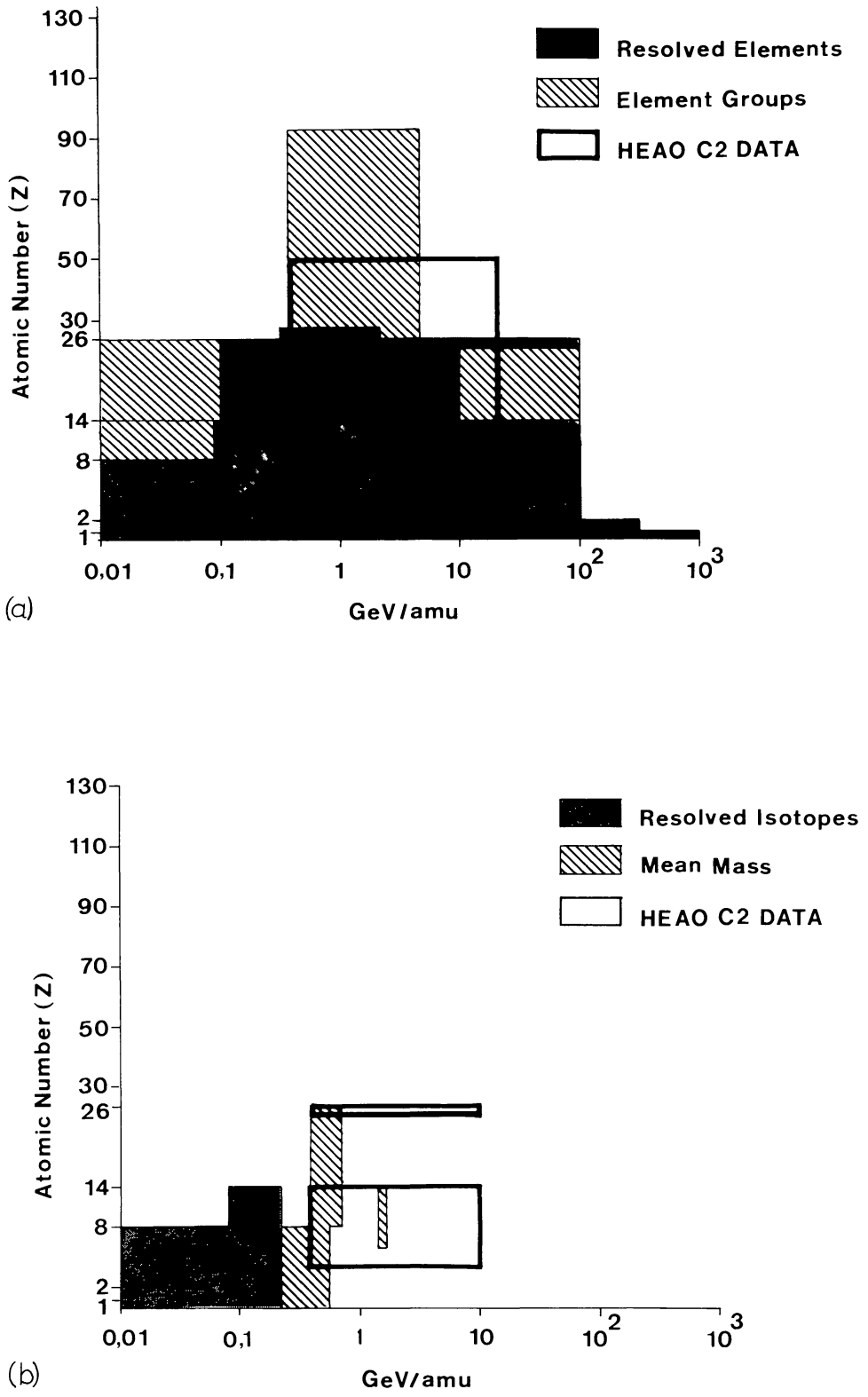

Fig. 1. Present Status of Cosmic Ray Composition Measurements and Data to be expected from HEAO-C2. (a) Charges. (b) Isotopes.

- Abundance ratios of all elements from beryllium to tin in the energy range of 0.5 to 25 GeV/nucleon;
- Energy variations in the abundance ratios of the elements in the energy range 0.5 to 25 GeV/nucleon.

Particular emphasis has been given to the abundance determinations in the iron group as this can give important clues about the sources of cosmic rays. It has long been thought that the explosions of massive, highly evolved stars are the sites of cosmic ray acceleration as well as of nucleosynthesis. Cosmic rays should according to this picture be a sample of matter created in connection with *r*-process synthesis and could, with proper regard to the contribution of interstellar material serve to verify or refine the current theories on stellar evolution and the origin of the elements [6, 7]. The time delay between nucleosynthesis of the elements and their acceleration to relativistic energies may be determined from the elemental ratios between iron, cobalt and nickel [8], because Co-56 is a K-capture isotope, which decays at thermal energies, but is stable at high energies, where all the electrons have been removed.

In this study the isotopic composition will obviously provide a more complete information than the charge composition. In addition the isotopic composition is unaffected by the 'chemical' selection processes which have been discussed in connection with the observed elemental composition of cosmic rays [9].

The precise determination of ratios between primary and secondary elements will allow the determination of the changes in cosmic ray abundances caused by fragmentation during propagation. The containment of cosmic rays in the Galaxy can be determined from the abundances of long lived radioactive isotopes such as Be-10, Al-26 and Cl-36 which have half lives comparable to the time spent in interstellar space. These abundances will also contribute information on the possible existence of dense clouds surrounding the sources and of a cosmic ray halo surrounding the galactic plane. Furthermore it should be possible to determine whether acceleration and propagation are simultaneous or subsequent processes [10, 11].

The evaluation of the propagation effects relevant for the data obtained by the present instrument will be facilitated by the fact that the spallation cross-sections are nearly energy independent in the relativistic energy range [12–14].

The energy resolution of the experiment will also allow the search for energy dependent features in the elemental ratios. This search could provide the first indication of individual cosmic ray sources [15, 16].

The composition of the cosmic rays might thus show the existence of individual sources, which are not discernible from the arrival directions of the particles due to their interaction with the galactic magnetic field.

3. Experimental Method

The telescope consists of 5 Cerenkov detectors and a flash tube hodoscope with 4 trays as shown in Figure 2. The hodoscope serves the dual purpose of allowing

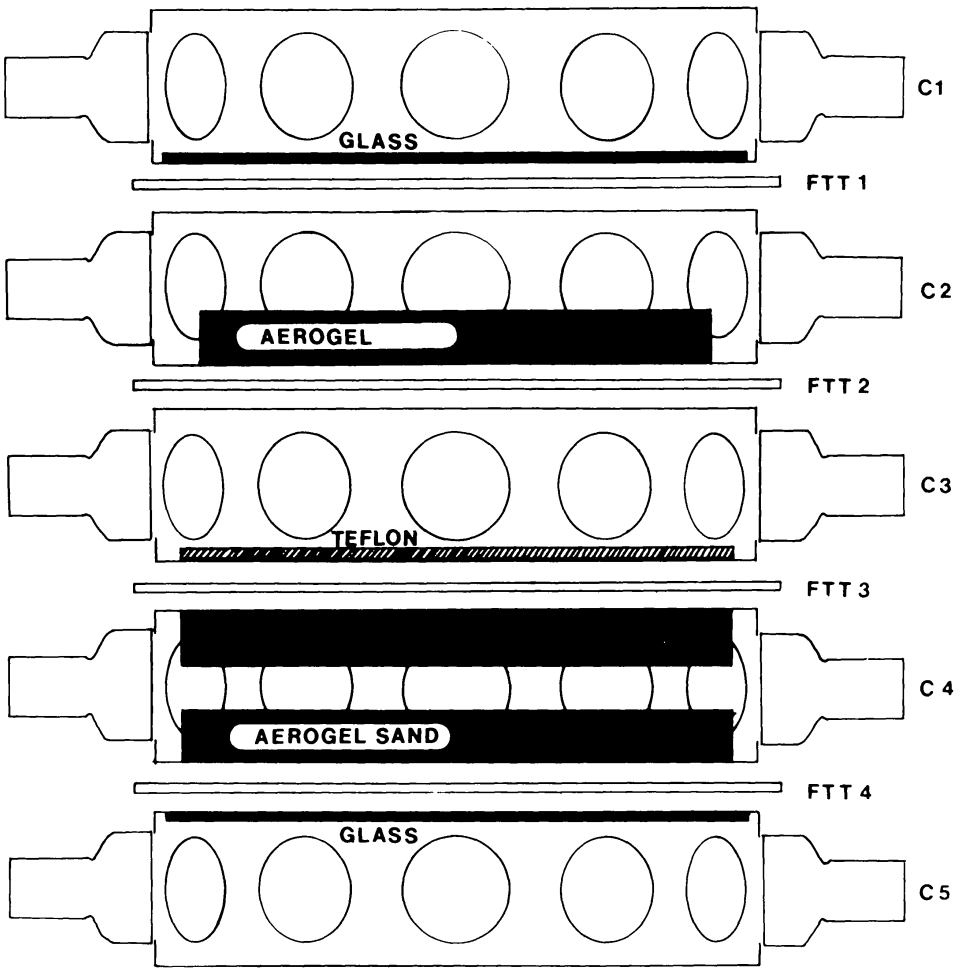

Fig. 2. The HEAO-C2 detector configuration, C1–C5 Cerenkov counters, FTT1–FTT4 flash-tube hodoscope.

corrections for geometrical variations in the Cerenkov counter response and to determine the particle trajectory in the geomagnetic field. The position of the experiment in the HEAO-3 satellite is shown in Figure 3. Both ends of the telescope are open to space and particles from both front and back will be analysed, their direction through the instrument being determined by a time-of-flight measurement.

The method of using a combination of Cerenkov counters with different refractive indices to determine the charge and energy of the particles traversing the instrument was first tested in a series of balloon flights in 1968–70. A simple telescope with two small Cerenkov counters demonstrated that a detector of this type was capable of measuring the flux of primary cosmic ray nuclei and to identify unambiguously each element up to at least $Z = 30$ [1, 17]. Since 1973 a series of balloon flights has been carried out with a larger instrument to test the performance of the counters and the hodoscope developed for the satellite instrument.

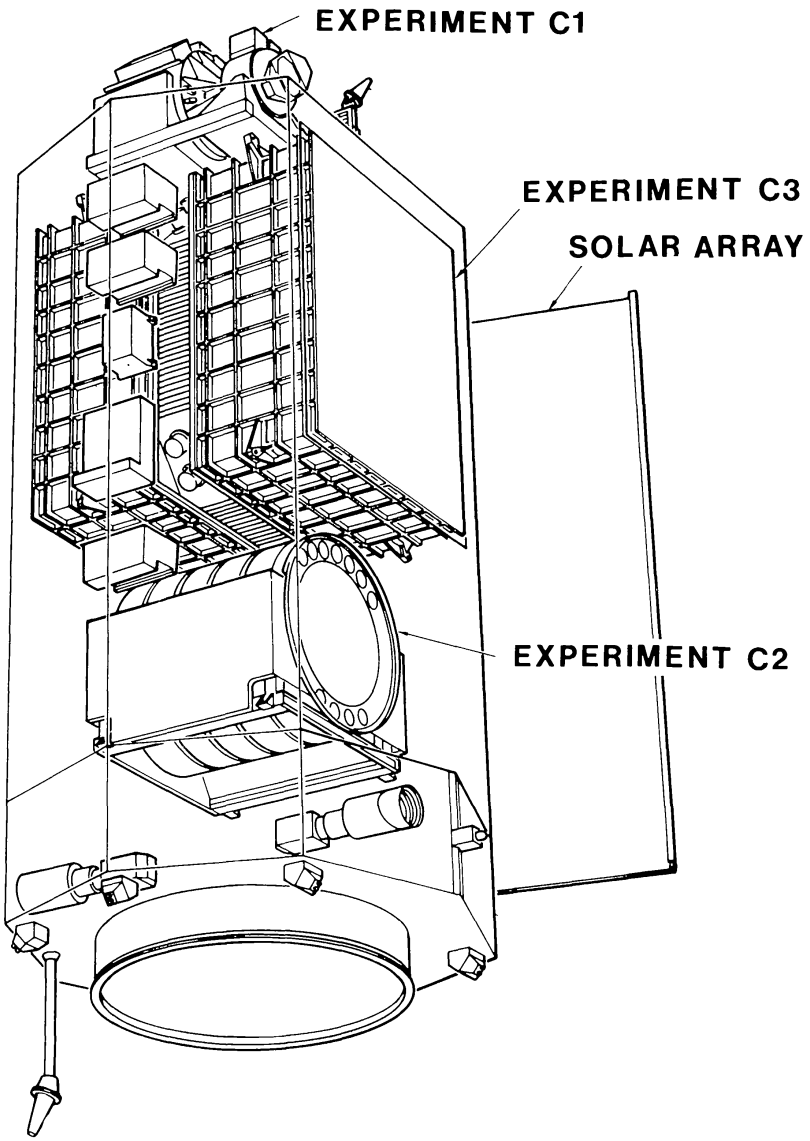

Fig. 3. The position of the C2 instrument in the HEAO-3 satellite.

The relation between the Cerenkov signal S in a single counter and the particle momentum/nucleon P can be written as

$$S = q_0 Z^2 \left(1 - \frac{P_0^2}{P^2}\right), \tag{2}$$

where q_0 is the light yield from a singly charged particle with velocity equal to the speed of light in vacuum, and P_0 is the threshold momentum/nucleon, given by

$$P_0^2 = \frac{1}{n^2 - 1}, \tag{3}$$

where n is the refractive index of the counter medium.

Combining the signals S_1 and S_2 from two Cerenkov counters with different

threshold momenta (P_1 and P_2) one can by eliminating P determine Z from

$$Z^2 = \frac{1}{q_0} \frac{P_2^2 S_1 - P_1^2 S_2}{P_2^2 - P_1^2} \tag{4}$$

assuming the counters to have the same response q_0 to a singly-charged relativistic particle.

Assuming photoelectron statistics to be the dominating cause of the fluctuations in the signal, we can determine the uncertainty of the charge resolution

$$\mathrm{d}Z \leqslant \frac{1}{2\sqrt{q_0}} \frac{\sqrt{P_2^4 + P_1^4}}{(P_2^2 - P_1^2)} = \frac{1}{2\sqrt{q_0}} K\,, \tag{5}$$

where K is between 1 and 2 for the combinations of refractive indices used in this experiment. Note that formula (5) is valid for any set of two counters. In the HEAO instrument the charge is determined by two or three independent sets. Once the charge is known, the particle momentum can be determined and under the same assumption the momentum resolution is given by the relation

$$\frac{\mathrm{d}P}{P} = \frac{1}{2Z\sqrt{q_0}} \frac{P}{P_0} \sqrt{\frac{P^2}{P_0^2} - 1}\,. \tag{6}$$

From this equation it is readily seen that a Cerenkov counter has good momentum resolution when P is only a little larger than P_0. However the instrument must cover a range of momenta corresponding to the cut-off variation along the satellite orbit, i.e. from about 1 to 10 GeV/c per nucleon. Therefore we use a set of counters with different refractive indices which makes it possible to obtain good resolution over a large range of momenta.

From Equations (1) and (6) one sees that for a given rigidity R the mass resolution of the counters is given by

$$\mathrm{d}M = \frac{M}{P}\mathrm{d}P = \frac{M}{2Z} \frac{1}{\sqrt{q_0}} \frac{P}{P_0} \sqrt{\frac{P^2}{P_0^2} - 1}\,. \tag{7}$$

This formula shows that as $M \sim 2Z$ the momentum range over which a counter gives good mass resolution is independent of the charge of the incoming particle to first order. However, as discussed in Appendix A, there are other sources of signal fluctuations than the photoelectron statistics, so formula (7) is only an approximation.

From Equation (1) it can be seen that the simultaneous determination of R, P, and Z allows the mass M to be calculated. P and Z are determined directly by the instrument whereas R must be determined from the particle trajectory in the Earth magnetic field.

Several different schemes have been developed to utilize the geomagnetic field to determine the mass composition [3], an overview is given in Appendix B.

4. Technical Description

A photograph showing the modular design of the instrument is shown on Figure 4 and a block diagram is given in Figure 5.

4.1. Cerenkov counters and analog electronics

Each of the five Cerenkov counters consists of one or two radiators (of light transmitting but not necessarily transparent material) contained in a box lined with a white diffusing material (HAWP Millipore filter paper) and viewed by twelve 5″ photomultiplier tubes as shown in Figure 6. All the boxes have the same inside dimensions: 60 cm diam and 17 cm height.

The C1 and C5 radiators are made of heavy flint glass (F2 from Schott Glass, Jena, D.D.R.) with effective refractive index $n = 1.64$, diam 60 cm and thickness

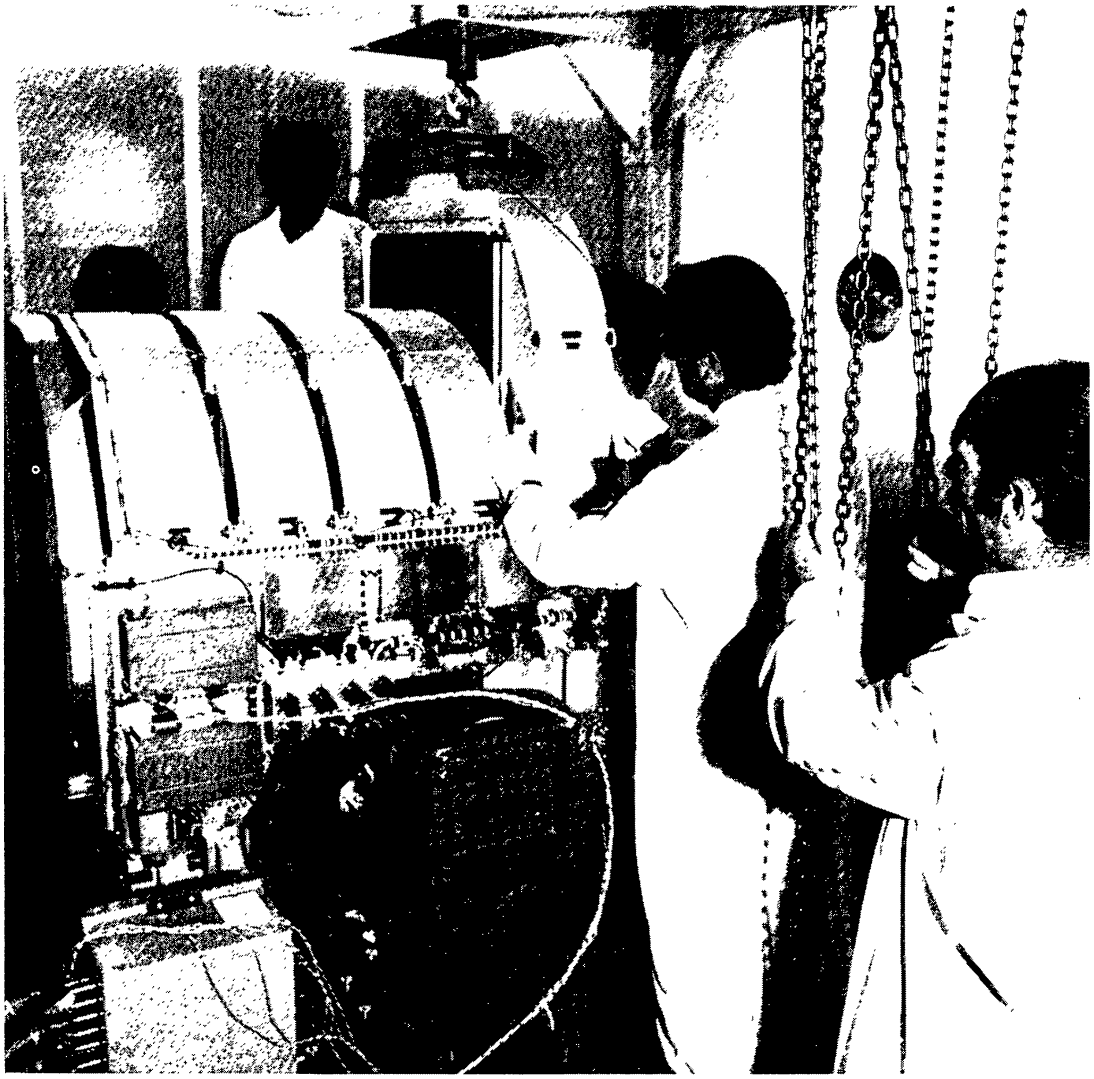

Fig. 4. Photo of the instrument during assembly.

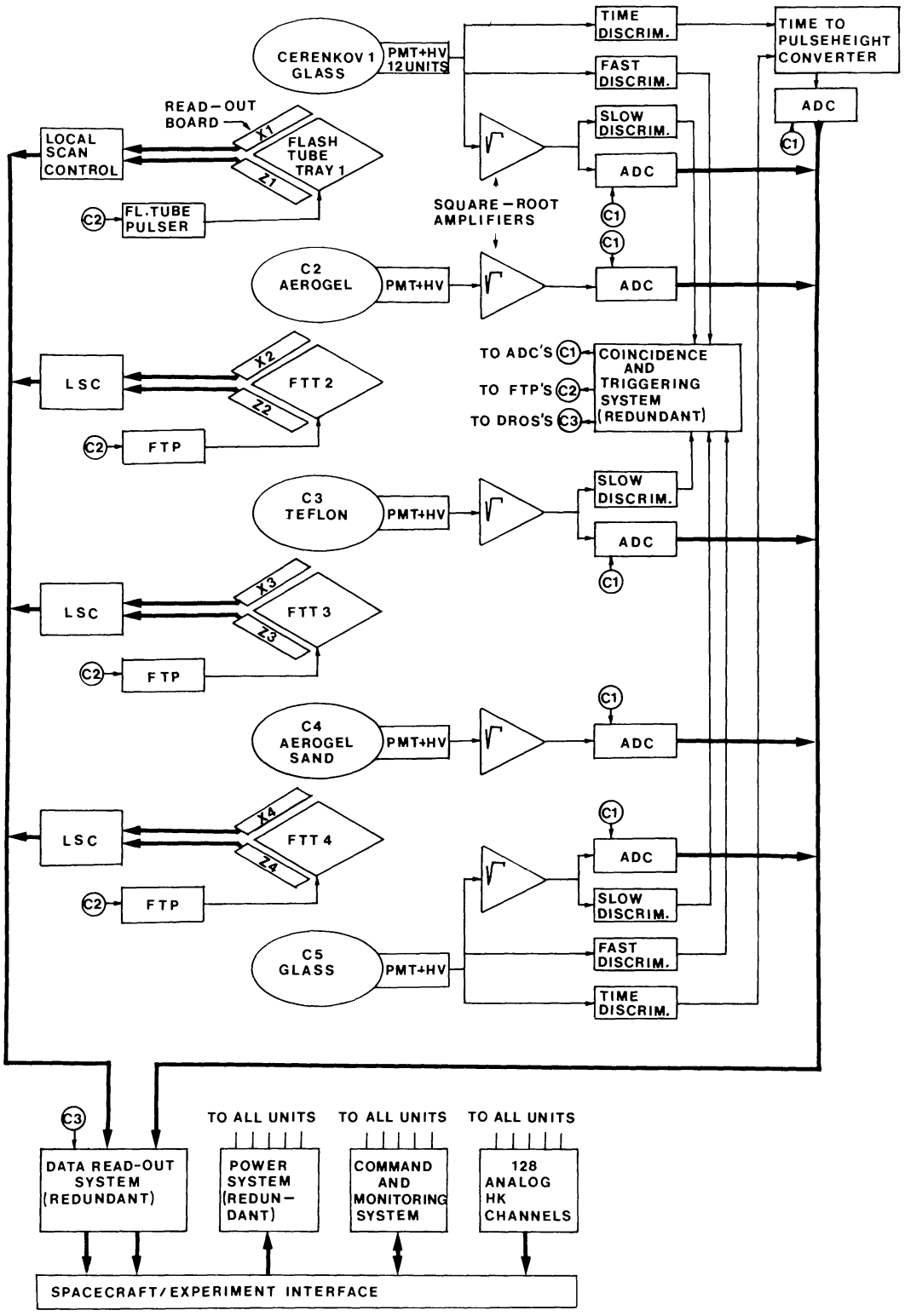

Fig. 5. Electronics block diagram of the HEAO-C2 experiment. Flash-tube high voltage pulser (FTP), pulse height analyzer (ADC), flash-tube read out control (LSC).

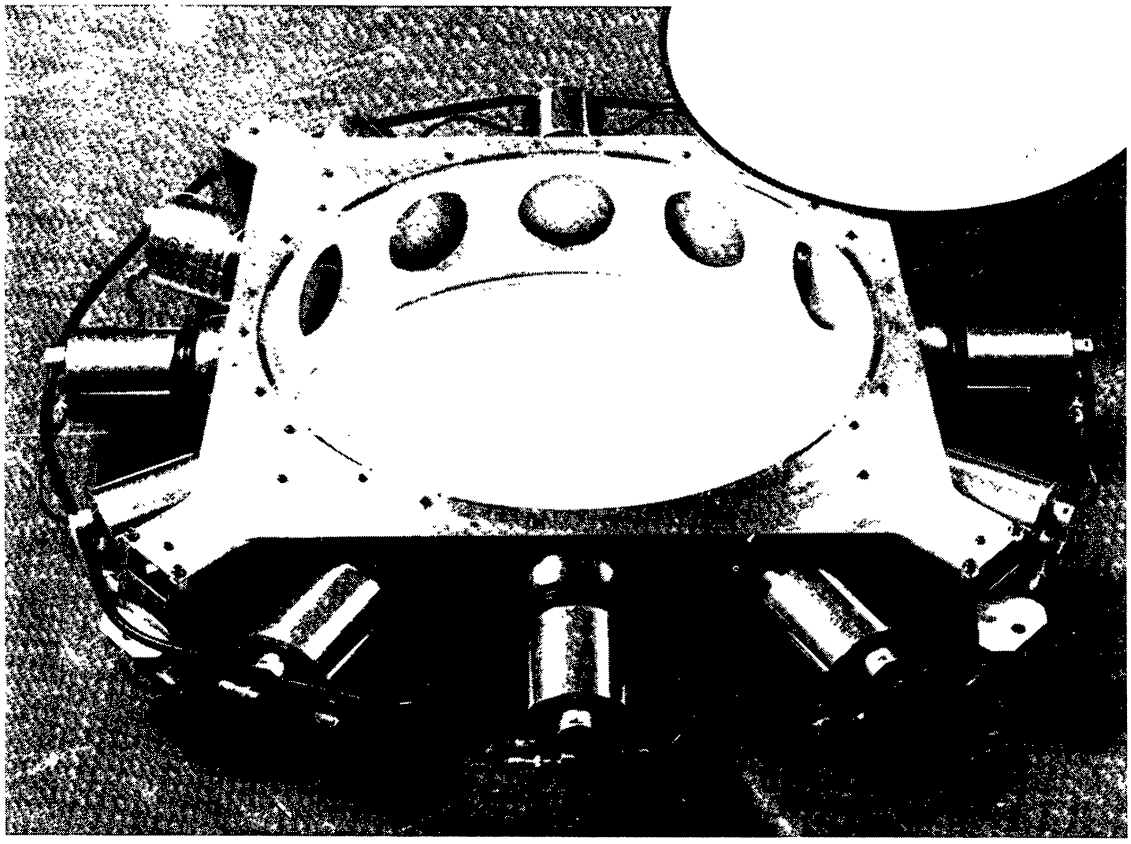

Fig. 6. The interior of a Cerenkov box showing the phototubes and the Millipore paper wall lining.

1 cm. They are sand blasted on the surface in order to reduce total internal reflection.

The C3 radiator is made of teflon (polytetrafluoroethylene). Its light output is consistent with Cerenkov light production in a medium with a refractive index $n = 1.33$, as measured with a beam of accelerated oxygen nuclei at the Lawrence Radiation Laboratory in Berkeley [18]. These measurements exhibited a response to nuclei below the Cerenkov threshold less than 3% of the maximum Cerenkov signal for fully relativistic particles.

The C2 and C4 radiators are made of different types of silica aerogel. These new Cerenkov radiators were developed during the HEAO project in order to match the momentum range to be covered in the HEAO-3 orbit. It was shown [19–21] that solid Cerenkov radiators with effective indices in the interval not covered by ordinary transparent materials can be produced using porous silica where the characteristic size of the inhomogeneities is small compared to the wavelength of the light to be detected.

The Cerenkov light output from the aerogel blocks is consistent with light production in a homogeneous medium with refractive index $n = 1.053$ as measured with relativistic neon nuclei at the Bevatron in Berkeley [22]. The amount of light below threshold was found to be about 2% of the maximum

pulseheight for fully relativistic particles. The above refractive index coincides with that measured at optical wavelength ($\lambda = 6328$ Å). The blocks are hexagons 15 cm across and 5.6 cm thick assembled in a mosaic with a 52 cm diam.

The silica aerogel with $n = 1.012$ is too fragile to be manufactured in the form of blocks. Therefore we used 'aerogel sand' consisting of grains with diameter in the range 1.6–3.2 mm. This size was chosen as a compromise between the homogeneity of response and the scattering of Cerenkov light at the boundaries of the grains [23]. Two radiators of aerogel sand are enclosed at the top and bottom of the same diffusion box as shown in Figure 2. The radiators are kept in place by mylar windows 36 μ thick.

The main characteristics of the five counters are summarized in Table I.

The ratio of effective photocathode area to total box area is 0.15. The photomultiplier tubes (PMT) are a special high reliability and ruggedized version (EMI 9791 NMA) of the standard 5″ tube 9709R. The photocathode is of the bialkali type with a quantum efficiency exceeding 20%. The set of PMT's used in each counter was matched to ensure that the spread of sensitivity was less than 2% and that the spread in temperature drifts was also within 2% for 10°C excursions from the nominal operating temperature. The gain of the 12 PMT's installed in their diffusion box was then adjusted using a rotating light emission device consisting of an alpha source (Am–241) coupled to a scintillator which ensures a good isotropy of the light emission. Final adjustment was made with cosmic ray muons. The gain adjustments were done by adjusting the high voltage power supply associated with each tube. During the flight it is possible to control by command the high voltage of each individual tube, setting it into one of 8 discrete steps covering a 100 V range around the nominal value or switching off the tube completely.

The sum of the charges collected by the anodes of the PMT's is voltage converted in one single preamplifier for each counter. The transfer curve (output voltage versus input charge) of the amplifier is a nearly perfect square root function over a dynamic range of 8000 from 2×10^{-13} C. The output pulse is routed to a level discriminator for triggering purposes and to a 10 bit analog-to-digital converter (ADC). Overall resolution of the system (preamp. + ADC) is

TABLE I
Cerenkov radiator characteristics

Counter	Radiator material	Refractive index	Density g cm^{-3}	Depth cm	Diam. cm	Light yield*
C1, C5	lead glass	1.64	3.61	1.0	60	40
C2	aerogel	1.053	0.255	5.6	52	14
C3	teflon	1.33	2.18	1.5	58	24
C4	aerogel	1.012	0.040	2×5.5	56	5

* Photoelectrons (for singly charged particles).

0.2% FWHM over the full range. The compression of the dynamic range achieved by the square root transfer curve ensures that the digitization errors are matched to the statistical fluctuations in the signals over the full signal range.

The C1 and C5 counters are also fitted with fast electronics. For these counters, the signals from the last dynode of the PMT's are added in two groups of six (odd and even numbered PMT's). The added output from each group is routed to a fast level discriminator for the use in the event trigger electronics. The two outputs from each counter are added and routed to a time discriminator (constant fraction of maximum amplitude) which delivers a start signal (C1) and a stop signal (C5) to the time-of-flight encoder. The time encoder has 0.5 ns resolution, using first a time-to-amplitude converter and then a 64 channel ADC.

The time-of-flight data are used to determine the travel direction of the nuclei through the telescope.

4.2. COINCIDENCE AND EVENT TRIGGER ELECTRONICS

The dead time of the instrument is normally determined by the dead time of the flash tube system, although the telemetry link capacity also can be a limiting factor. It is therefore important that the event trigger system can discriminate against the most common types of background events and only allow the flash tube system to be fired for 'good' events.

The trigger system must be able to reject the following types of events:
- Events outside the useful geometry (important because of isotropic flux);
- Events undergoing a nuclear interaction during the traversal of the instrument (important because of the large amount of matter in the path of the particles);
- Events with charge 1 and 2 (important because hydrogen and helium are more than 99% of the total flux).

In our system the trigger pulse is generated from the coincidence between a 'slow' signal and a 'fast' signal.

The slow signal is generated as a triple-coincidence between signals from discriminators associated with C1, C3, and C5. The fast signal is generated as a four-fold coincidence between signals from discriminators connected to the odd and even PMT groups on C1 and C5.

The trigger pulse is thus the result of a seven-fold coincidence as shown in Figure 7. Each of the 7 level discriminators can be individually adjusted in four steps or completely removed from the coincidence by command. The levels are adjusted so that the slow discriminators on the glass counter determine the charge threshold. The odd-even fast coincidence is used to remove particles passing through the PMT windows, outside of the useful geometry. The time resolution is ~100 ns for the fast coincidence pulse and 1 μs for the slow pulse.

When an event has satisfied the coincidence criteria the following triggering sequence is performed (assuming the system is not already busy):
- ADC start signals are issued first (also for the time-of-flight analyzer);
- A strobe is delivered to the Amplitude Ratio Discriminator (ARD) circuitry.

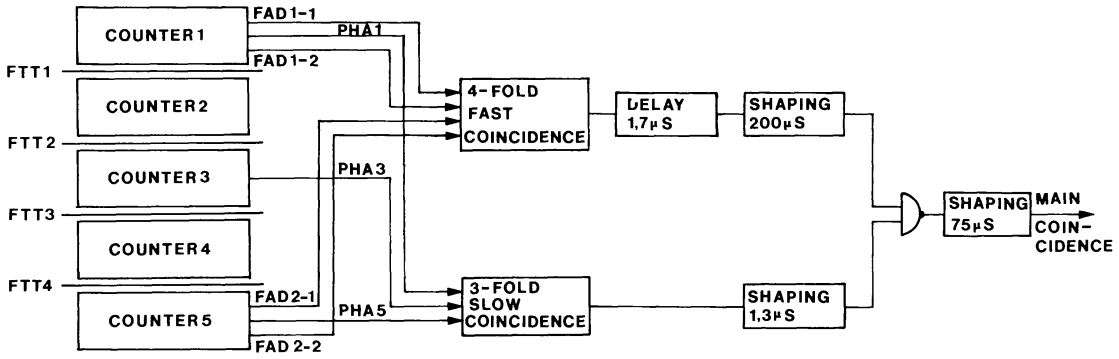

Fig. 7. Event trigger, fast–slow coincidence system.

This circuit compares the two glass counter signal amplitudes: if the ratio is outside preset limits, a veto flag is raised. Limits are ground selected from 10% to 30%. ARD function may be inhibited. The veto flag is never raised for nuclei with charge greater than 10. The purpose of the ratio discriminator is to inhibit the use of the flash tube system on events in which nuclear interactions have taken place. The effect is shown on Figure 8;

- Unless a veto flag is present, the flash tube high voltage pulsers are fired. The firing occurs with a delay determined for each event from the C1 and C5 output pulses. The purpose of this delay will be explained in Section 4.3. The minimum delay is 1.8 μs (for $Z = 3$), the maximum delay ranges from 14 to 27 μs (for $Z = 50$); this value depends on the command status;
- Finally the data read out system is triggered.

The useful geometry is 0.07 m^2 sr for each direction of propagation. The useful geometry is defined by the top cover of C1 and bottom cover of C5 (see Figure 2). The trigger geometry is of course larger. The maximum angle of incidence for the useful particles is 31°.

The total amount of matter traversed by particles propagating parallel to the telescope axis is 16.7 g cm^{-2}. The proportion of incident particles interacting within the telescope is about 30% for Be, 38% for O and 54% for Fe nuclei.

In the flight configuration particles are detected if they trigger the fast and slow discriminators of C1 and C5 set at 6 q_0 (where q_0 is the signal given by singly charged relativistic particles) and the discriminator of C3 set at 2 q_0. The charge threshold is therefore $Z = 3$ and the energy threshold is determined by the requirement that particles trigger the teflon counter. When entering the telescope such particles will have a minimum energy of: 520 MeV/n for Be, 550 MeV/n for O, 580 MeV/n for Si and 635 MeV/n for Fe nuclei. The upper limit of measurable charge is 50.

4.3. HODOSCOPE AND ASSOCIATED ELECTRONICS

The flash tube system consists of four trays, each of which contains two layers of flash tubes, allowing the determination of the X- and Z-coordinates of the

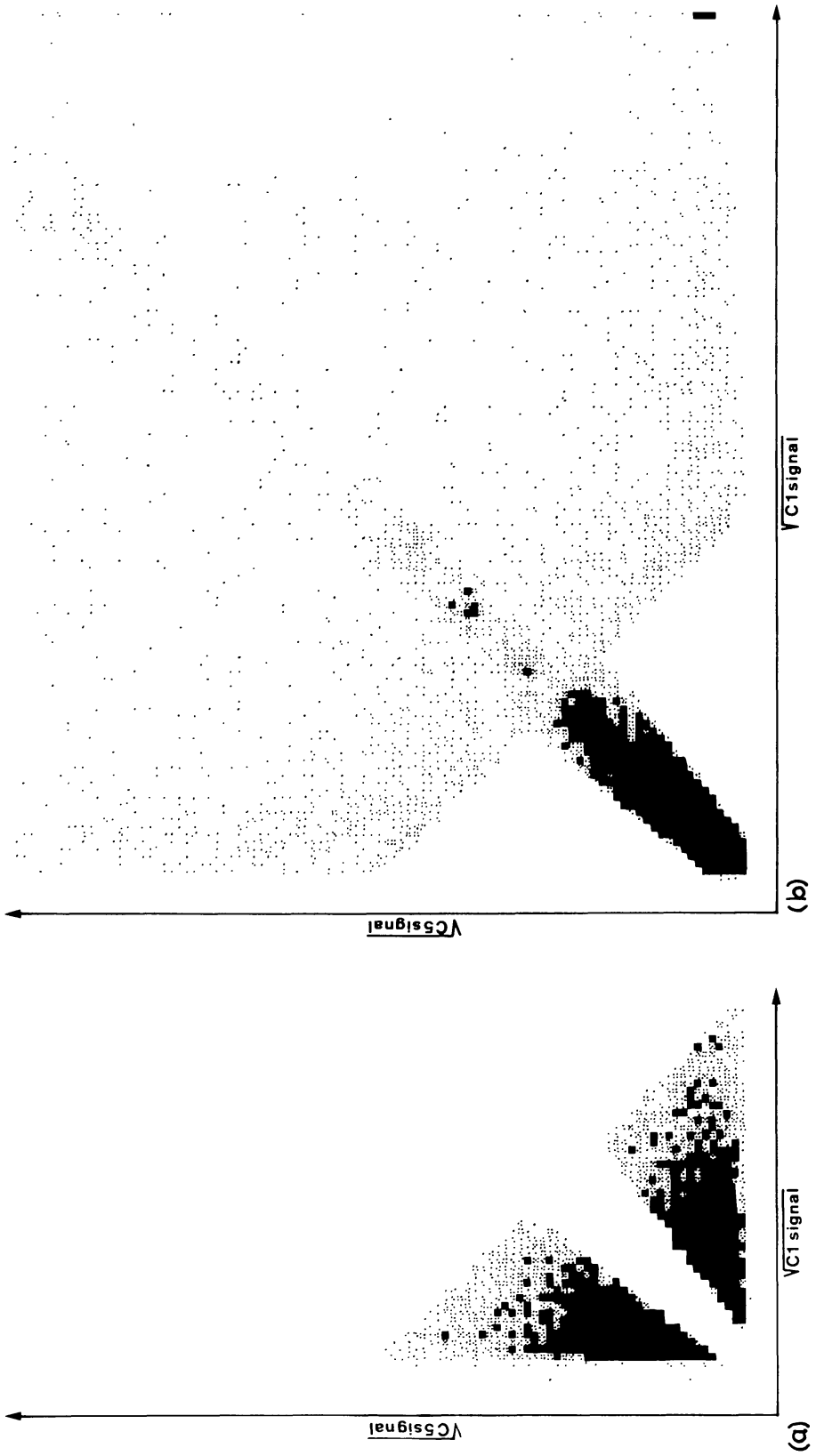

Fig. 8. Effect of the amplitude ratio discriminator (ARD) circuit. (a) Events rejected by ARD flag. (b) Events accepted.

particle impact point in the tray plane. The two layers are placed between three titanium plates of which the central one is used as a high voltage electrode and the two outer ones act as ground planes (see Figure 9). The trays are located in the space between the Cerenkov boxes. The active area of the flash tube trays (600×600 mm) is sufficient to ensure that all particles passing through the Cerenkov counters will pass through all four trays. Each layer of flash tubes contains 128 glass tubes, 670 mm long with outer diameters of 4.85 mm and nominal wall thickness of 0.2 mm. The tubes are selected from commercially available glass tubing (GW-tubes, Glasswerk Wertheim, Germany). The tubes are filled with neon at atmospheric pressure with 0.2 torr of H_2 and 0.1 torr of O_2 added.

When a charged particle passes through a flash tube, it will ionize the gas molecules along the trajectory. If no high voltage pulse occurs the ions and electrons will recombine in a few microseconds. However, if a high voltage pulse is applied across the tube before recombination takes place, the liberated electrons will start an avalanche which in turn will grow into a glow discharge filling the interior volume of the tube. Wall charge effects cause the discharge to terminate itself in about 1 microsecond. An outside electrode at the end of each tube can detect the discharge through capacitive coupling with the plasma in the tube. The tubes are painted black on the outside to prevent the spreading of the discharge from tube to tube via the liberated UV-photons.

When a charged particle traverses the instrument, numerous high energy electrons may be projected away from its path. These electrons could trigger many of the tubes far away from the primary track, thereby reducing the probability of locating the track correctly. A significant reduction in the appearance of such unwanted flashes can be achieved by delaying the high voltage pulse with respect to the particle passage. During the delay time ion-electron recombination will take place thereby neutralizing the majority of the tubes hit by the knock-on electrons, while the tubes traversed by the heavy particle will still be partly ionized due to the much higher initial ionization. We use a variable delay determined from the signal in the glass Cerenkov counters, to optimize the

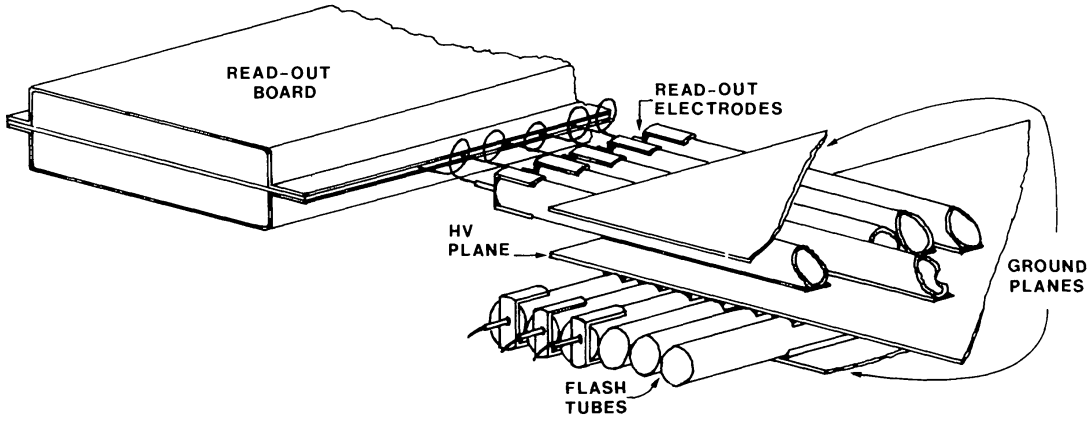

Fig. 9. Flash-tube tray.

suppression of the electron induced flashes, while retaining a high efficiency for the detection of the primary particle [24, 25].

Each flash tube tray is connected to a high voltage pulse unit, which provides a pulse with a nominal peak voltage of 3.2 kV. This voltage can be adjusted by command to one of four levels between 2.4 and 3.5 kV. Each flash tube tray can be removed from the triggering sequence by disabling the associated high voltage unit.

The recharging time of the high voltage pulse units determine the dead time of the instrument. The pulsers have been designed to handle continuous triggering rates up to 12 Hz, and through the use of an internal capacitor energy storage it has been possible to allow triggering of the units twice within a 20 ms interval or three times within 50 ms.

1 μs after the application of the high voltage pulse a strobe pulse is sent to the two readout boards associated with each flash tube tray and the signal pulse on the electrodes of the fired tubes are used to set a flip-flop. The state of the flip-flop registers are later interrogated by the data readout system.

4.4. DATA READOUT SYSTEM

In order to make efficient use of the telemetry words an elaborate data formatting system has been included in the instrument (see Figure 10).

The arrival of cosmic ray particles is randomly distributed in time; many particles pass through a phototube or undergo nuclear interactions during the passage through the instrument and the number of flash tubes triggered varies from event to event. This means that the amount of data collected fluctuates strongly in time whereas the data output from the experiment to the spacecraft is at a constant rate of 60 science data words every major frame (40.96 s).

Our approach to ensure efficient use of a fixed number of words to transmit a variable amount of data is based upon:

1. On-board classification of events into 'good' and 'bad'.
2. Three different formats (see Figure 11). A short and a medium format used to transmit 'bad' events and a long format of variable length used to transmit 'good' events.
3. A double buffer system where the events are stored next to one another (i.e. empty words between events are eliminated).

This approach means that in fact we have established our own variable, floating format within the fixed satellite telemetry format.

The data generated by the instrument consists of:

5 Cerenkov counter signals (5×10 bits);
1 Time-of-flight signal (8 bits);
1 Flash tube delay monitor signal (8 bits);
1 Event arrival time (8 bits);
N Flash tube addresses ($N \times 10$ bits, $N < 44$);
1 Number of flash tubes fired (6 bits);
2 Flags (2 bits).

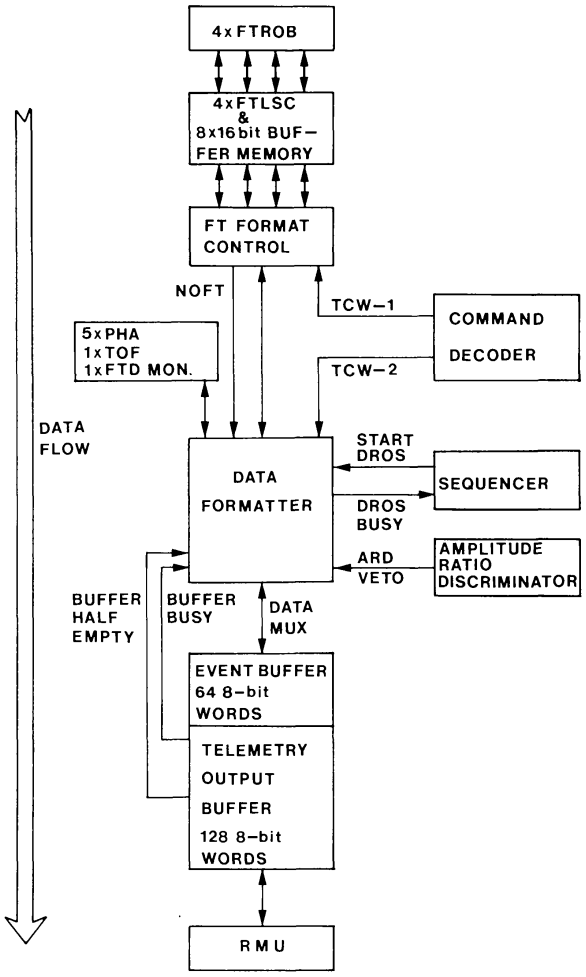

Fig. 10. Block diagram of the Data Read Out System (DROS).
FTROB = Flash Tube Read Out Board.
FTLSC = Flash Tube Local Scan Control.
NOFT = No. Of Flash Tubes fired.
TCW = Telemetry Command Word.
PHA = Pulse Height Analyser.
TOF = Time-of-Flight.
FTDMON = Flash Tube Delay Monitor.
RMU = Satellite Remote Multiplexing Unit.

The events are time tagged to an accuracy of 32 ms to allow reconstitution of the precise spacecraft attitude and position during data analysis.

A 'bad' event is recognised on-board from flags indicating a disparity between the signals from the two identical counters C1 and C5 or by the presence of unusually many flash tube readouts from the event (the condition for the raising of the flags can be controlled via command). Rather than suppressing the 'bad' events completely, just enough information about each is transmitted so the on-board selection scheme can be monitored and its validity verified.

The choice between short or medium format is based upon the amount of data already stored in the instrument telemetry buffer, the short format is used when the buffer is nearly full.

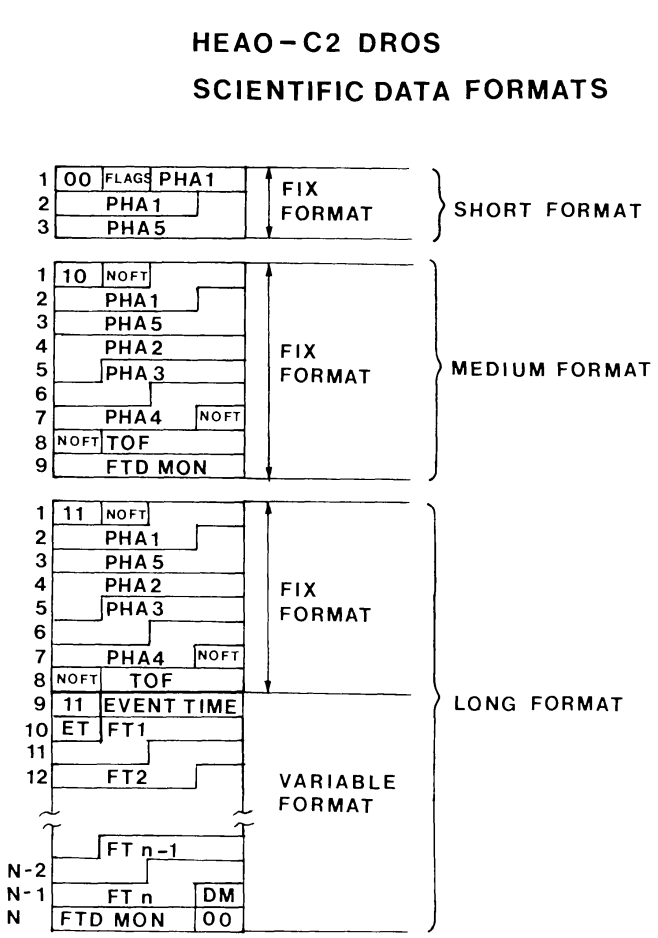

Fig. 11. The three science data formats.
PHA = Pulse Height Analyser.
NOFT = No. Of Flash Tubes fired.
TOF = Time Of Flight.
FTDMON = DM = Flash Tube Delay Monitor.
ET = Event Time.

The data is stored in three different buffer levels during the on-board processing of an event. Immediately after the trigger pulse the digitized data are placed in local registers associated with the ADC's and the flash tube read-out boards. Thereafter the data are collected, formatted and stored in the event buffer. This buffer is 64 8-bit words deep and this buffer size limits the maximum number of flash tube addresses to 43. The event buffer will only hold one event at a time irrespective of the actual event length.

The event is moved down into the telemetry output buffer when there are enough free words in this buffer. To ensure that the move does not coincide with a data output request from the satellite telemetry system the event move is synchronized with the telemetry output. The new event is moved so far down into the output buffer that the beginning of the event follows right after the end of the previous event.

The size, 128 8-bit words, of the telemetry output buffer makes it capable of holding several events (typically six 'good' events of 200 bits average length plus six 'bad' events of 64 bits fixed length). The length of the buffers is determined by consideration of the maximum acceptable event lengths and by the available integrated circuit memory elements. Buffers of this length have been verified to adequately smooth out the random data 'production' such that little time will be lost while waiting for the telemetry channel to clear (see Figure 12).

The recovery of the internal synchronization during data analysis on ground has turned out to take place very quickly after each data error. The ascending sequence of flash tube addresses serves as a synchronization mark (the chance occurrence of N words in ascending order is $1/(N!)$).

The telemetry rates are 1.6 kbits/s of science data and 50 bits/s of housekeeping data. There are 112 analog channels, 80 bits of command status information and 72 count rates transmitted during each major frame (40.96 s).

4.5. INSTRUMENT RELIABILITY AND TESTING

During instrument design great care was taken to reduce the probability of loss of the entire experiment through single point failures, this goal was achieved through the use of redundancy in the design.

The limit set for definition of 'instrument failure' was 50% loss of scientific value. The flash tube system is fully redundant: 3 trays out of the four are sufficient for straight line reconstruction. If one of the counters fails, only part of

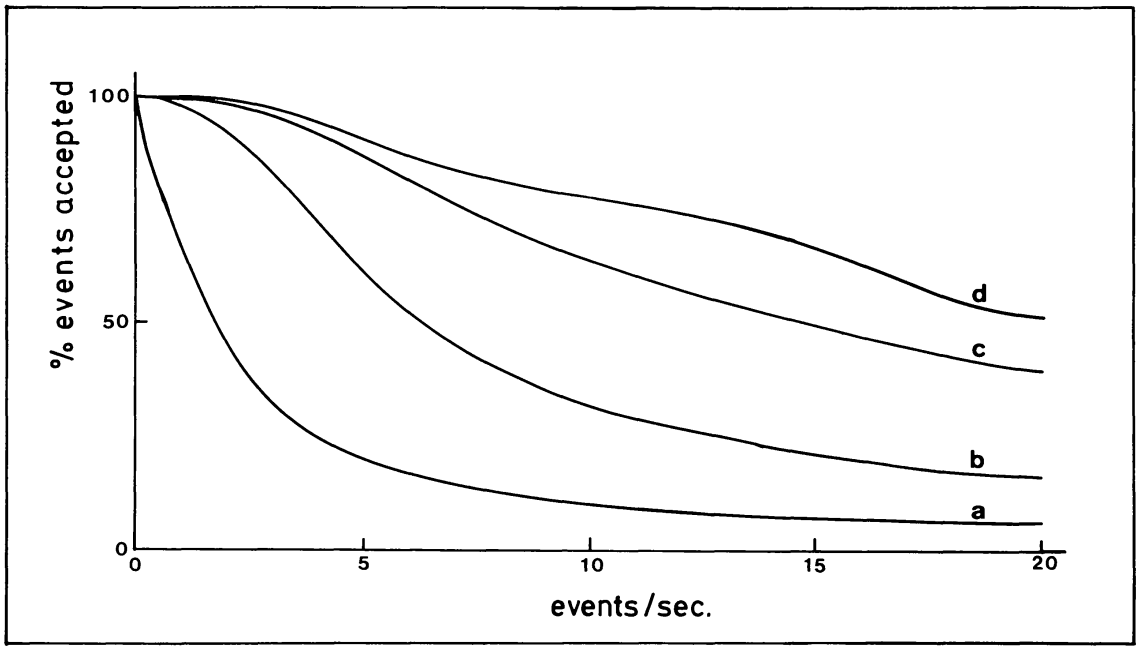

Fig. 12. Events accepted as a function of counting rate. Four different read-out systems: (a) Fixed length format, fixed position, no buffer. (b) Fixed length format without buffer. (c) Variable, floating format without buffer. (d) Variable, floating format with buffer (as used).

the events disappear from the data: around 30% for the velocity counters, and 40 to 50% for glass counters.

The inherent redundancy of the detector telescope is preserved by providing 60 individual high voltage supplies for the PMT's, separate analog chains to each Cerenkov counter and separate encoding electronics to each flash tube tray.

All other subsystems are redundant:

- Two low voltage converters (stand-by redundancy);
- Two trigger systems (stand-by redundancy);
- Two data read-out systems (each of them handles half of the data);
- Command system: each of the 8 serial command words are processed in the instrument by independent circuits while individual commands are distributed to minimize the impact of one command word failure.

Also, a number of design precautions have been implemented to prevent failure propagation:

- Power distribution through fuses or active current limiters;
- Protection resistors and diodes at all interfaces between subsystems.

The total number of electronic parts used in HEAO-C2 is about 15 000. This means that there are more than 60 000 solderings in the instrument. Parts were selected from ESA, CNES and NASA–MSFC preferred part lists. Special emphasis has been paid to the reliability of the 60 PMT's. The PMT's '9791 NMA', 5″ bialkali photocathode, were purchased from EMI (England) who developed a computerized test bench and special procedures, under NASA–MSFC and CEA requirements. For this order, EMI initially manufactured 200 tubes. After screening, aging and fatigue testing, 104 were delivered to CEA, among which 72 tubes were selected for flight and spares.

During more than 2400 h of operation (including 1200 h in orbit) the gain drift on the tubes has been less than 3%. The 60 PMT high voltage supplies are completely potted (except for the low voltage sections) and were tested individually for corona at all pressures from ambient down to 10^{-6} torr.

The 4 flash tube high voltage pulsers are designed with an open structure using only conformal coating. The flash tube trays also use an open structure design. The flash tube system is only qualified for pressures lower than 10^{-3} torr. This means that a 48 hr outgassing period was required before switching on the flash tube high voltage in orbit.

All other electronics are double-sided conformal coated printed circuit boards, the integrity of which is maintained by using very light and very rigid honeycomb boxes. Each box is an independent module performing a single function. This design philosophy has shown great flexibility during integration tests and maintenance and modification of the system. Consequently wiring harness complexity has never turned out to be a problem.

All units were electronically tested before integration. All parts of the flash tube system were also submitted to vibration tests and thermal vacuum tests. In addition one flash tube tray was submitted to an acoustic test.

After the instrument was finished, it underwent a series of calibrations and functional tests. This was done with the use of computer controlled ground support equipment, which was also used later when the instrument was integrated in the satellite. Before integration the completed instrument was subjected to a full 3-axis vibration test and a thermal vacuum test.

5. Experiment Performance

HEAO-3 was launched at 05:28 UT on September 20, 1979 into a circular orbit with an altitude of 496 km and an inclination of 43.6 degrees. The orbital period is 94.6 min. The period of revolution of the satellite is 20 min.

The turn-on and adjustment phases lasted nearly 4 weeks and the experiment was commanded into its final configuration on October 16, 1979. All detectors and electronics were functioning nominally.

Preliminary results have been obtained from the quick look data during the 3 first months of orbital life.

During that period, the experiment temperature remained quite stable at 15 ± 2 °C. After correcting the counter signals for the effect of these slight temperature variations, long term drift can be estimated by using the peak positions of C and O nuclei. The drift of the counters was less than 3% over this three month period. To avoid degradation due to radiation damage, the PMT tubes are switched off during all South Atlantic Anomaly passages. When switched on, they recover their normal gain in less than 2 minutes.

The hodoscope efficiency depends on the charge of the particle: it is about 65% for B nuclei, 90% for O nuclei, and 95% for $Z > 14$. To estimate this efficiency, we took advantage of the overdetermination of the straight lines in the 4-layer flash tube system, which allows the determination of the efficiency of each layer independently. The system efficiency was then deduced from the efficiencies of the individual layers.

The time-of-flight system is performing well ($> 98\%$ correct direction assignments) for $Z > 6$. For the lowest charges the resolution is rather poor and direction information is only available for those lithium and beryllium nuclei which arrive on trajectories that later intersects the solid Earth. For these elements only 25% of the events can be assigned unique arrival directions. In Figure 13, raw and corrected time-of-flight data are presented.

Before analyzing the energy spectrum or isotopic composition, it is necessary to have sufficiently good charge resolution to avoid contamination of a rare chemical species by a more abundant element. The first step is to reject background events due to nuclear interactions produced in the instrument itself or in its neighbourhood. This is done by requiring consistency between the signals by C1 and C5, and single straight line events. Figure 14 shows the effect of the rejection of interactions using a strict amplitude ratio and the straight line data.

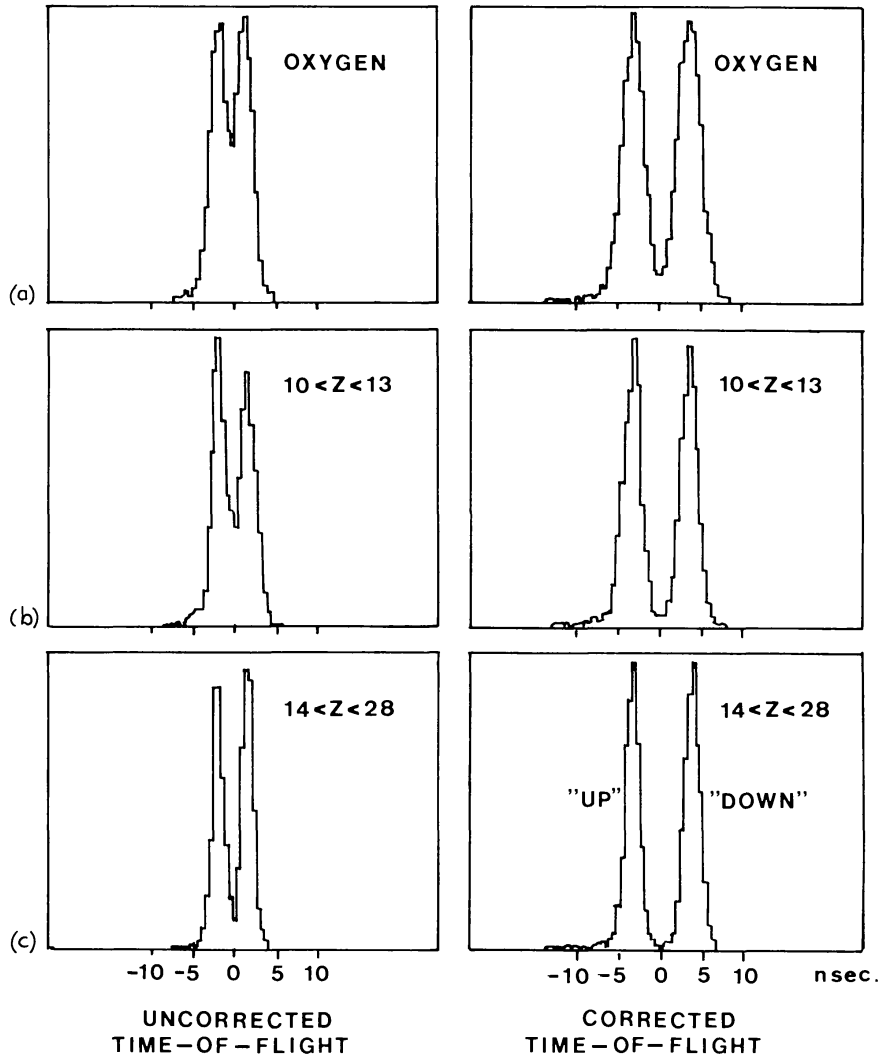

Fig. 13. Time-of-flight signal distribution for (a) Oxygen. (b) Neon to aluminum. (c) Silicon to iron. Raw data on the left, corrected data on the right. 'Down' direction is from C1 to C5.

The light collection efficiency varies slightly with the coordinates of the particle impact point on the radiator. Maps of this variation can be constructed by using selected nuclei such as C and O. Maximum variations are of the order of 3% between center and edge for glass and teflon radiators, and can attain 10% for aerogel radiators. Figure 15 shows such a map.

With the selected and corrected events, two-dimensional diagrams of signal combinations were used to determine the charge scale as function of particle velocity as shown in Figure 16. A more refined analysis results in charge histograms such as those presented in Figure 17. Above 2 GeV per nucleon the charge resolution, assuming gaussian distribution, is typically 0.11 charge unit for O and 0.15 charge unit for Fe nuclei, and varies slowly between these values for intermediate charges.

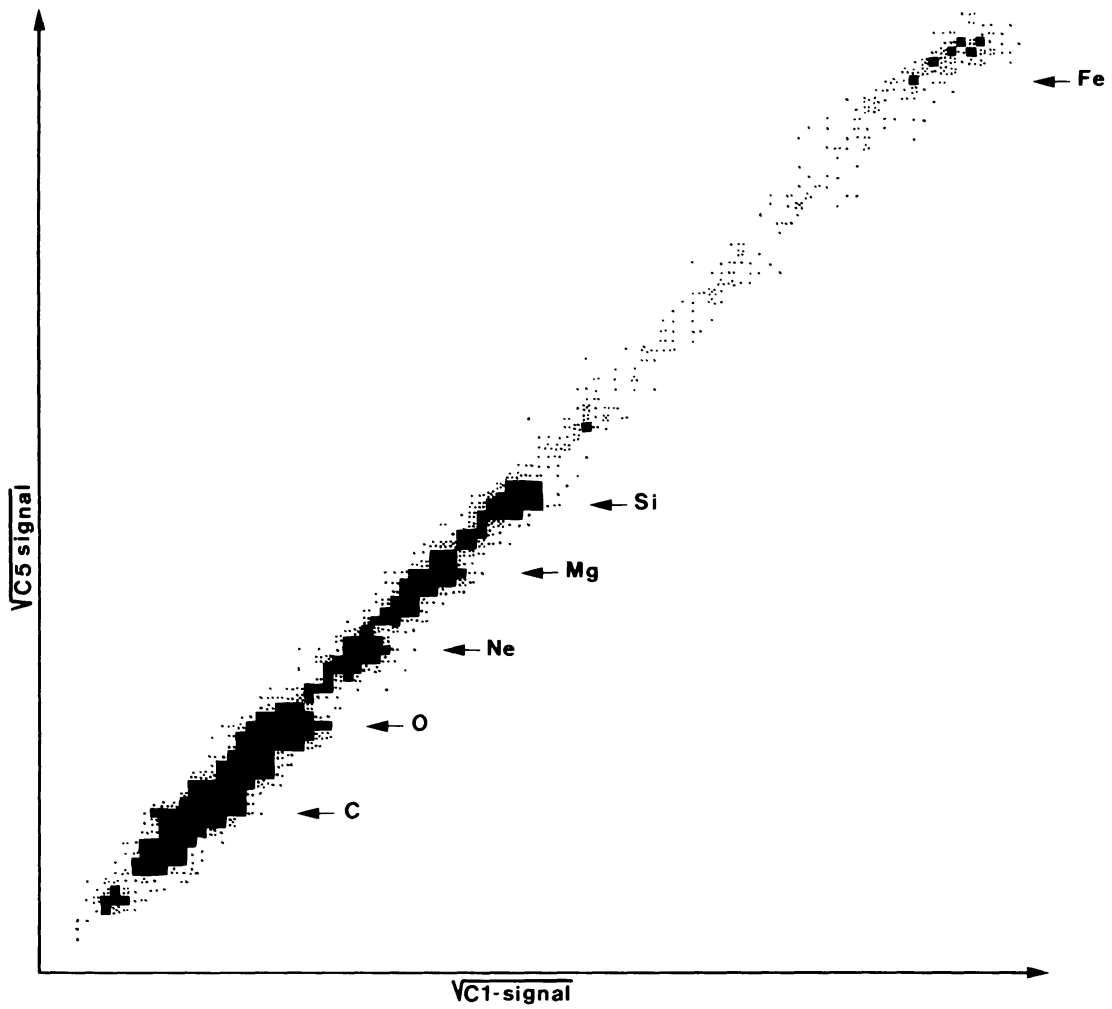

Fig. 14. Events accepted after interactions have been rejected by the requirement of a straight line in the hodoscope data and the use of a strict amplitude ratio (compare with Figure 8b).

Good charge resolution is achieved over the whole range of energies from 0.5 to 25 GeV/nucleon. This will allow us to determine the relative abundance of all elements up to charge 30; even the abundance of rare nuclei like Co, Cu, and Zn will be measurable.

The stable performance of the instrument has resulted in scientific data of a very high quality. The amount and quality of the data is far beyond any obtained in previous balloon experiments. The HEAO-C2 experiment should thus provide the basis for many important scientific discoveries.

Acknowledgements

The authors thank the following persons for their help over the years in preparing the C2 experiment: J. Lindner (assistant project manager at TRW), F. Speer (project manager at MSFC), W. Wilkinson (C2 experiment manager at

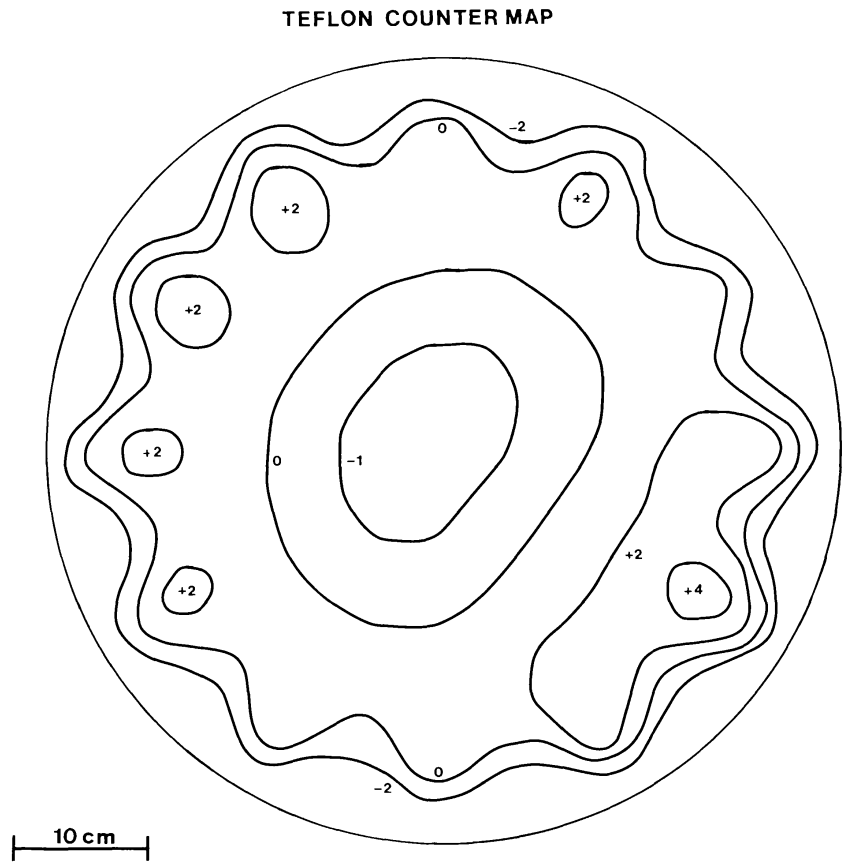

Fig. 15. Map of teflon counter showing geometrical effects in signal level. Numbers show percent deviation from average signal.

MSFC), T. Parnell (HEAO-C project scientist), H. Linder (GSFC programming support), G. Vincent (DRL support), F. Giordano (OCC manager), J. Seeback (experiment liason at OCC), H. H. Heckman, and H. J. Crawford (Bevatron support).

This work was supported in part by CNES contracts and by NASA with regard to Bevatron calibration and balloon flights over the years 1973 to 1978.

Appendix A: Momentum Determination from Cerenkov Signals

The signal from the Cerenkov counters can be considered to be composed of four different contributions:

(1) The direct Cerenkov emission of the incoming particle (The Primary Signal, discussed in the text);

(2) The Cerenkov emission from fast knock-on electrons (The Secondary Signal);

(3) The Cerenkov emission arising from the Millipore paper lining the inside of the counter boxes and, in the case of the aerogel counters, the Cerenkov signal from the mylar foils used to restrain the radiators in the boxes (The Foil Signal).

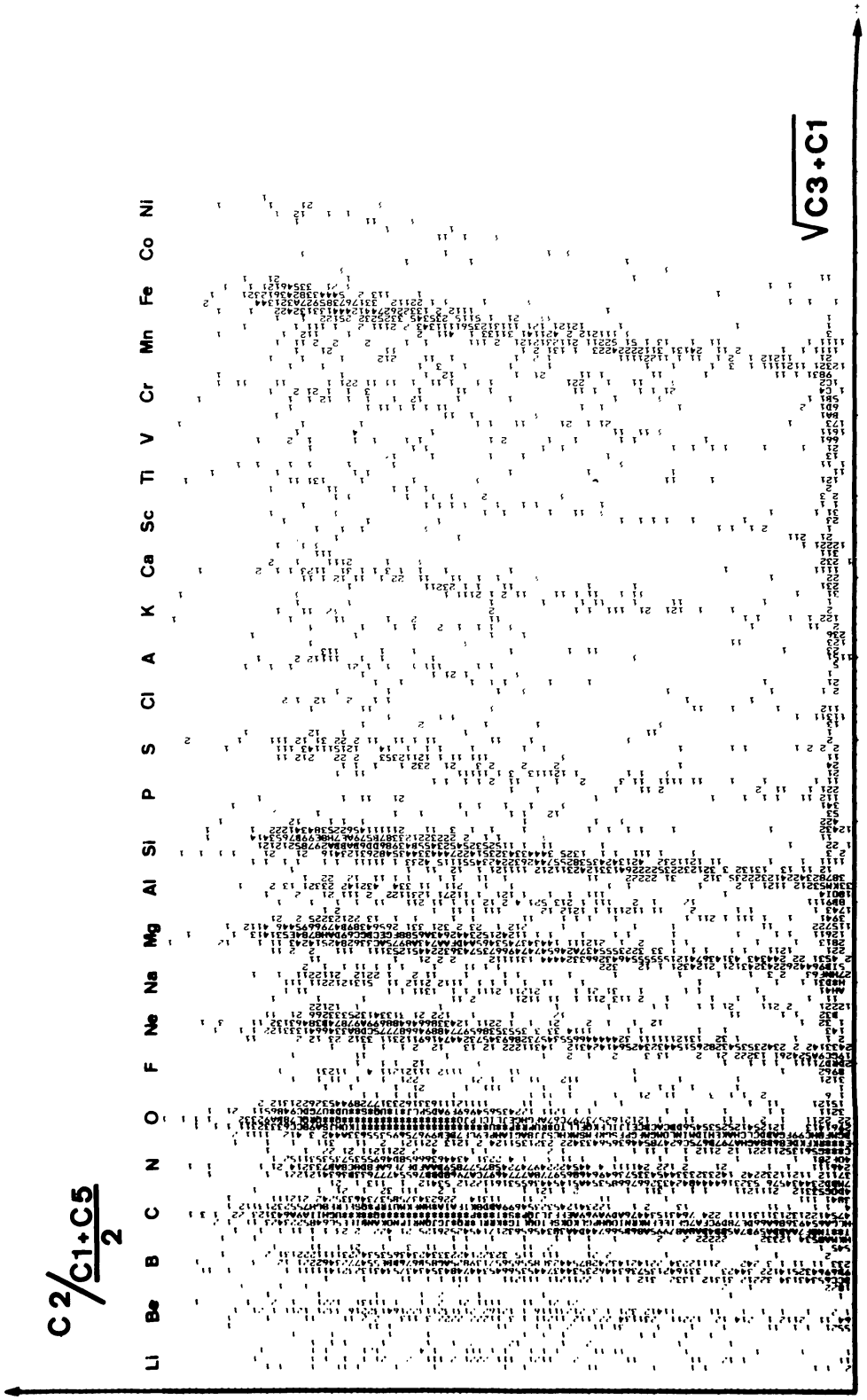

Fig. 16. Two dimensional plot of events in the region. $3 > Z > 30$. Geometrical and temperature corrections have been applied.

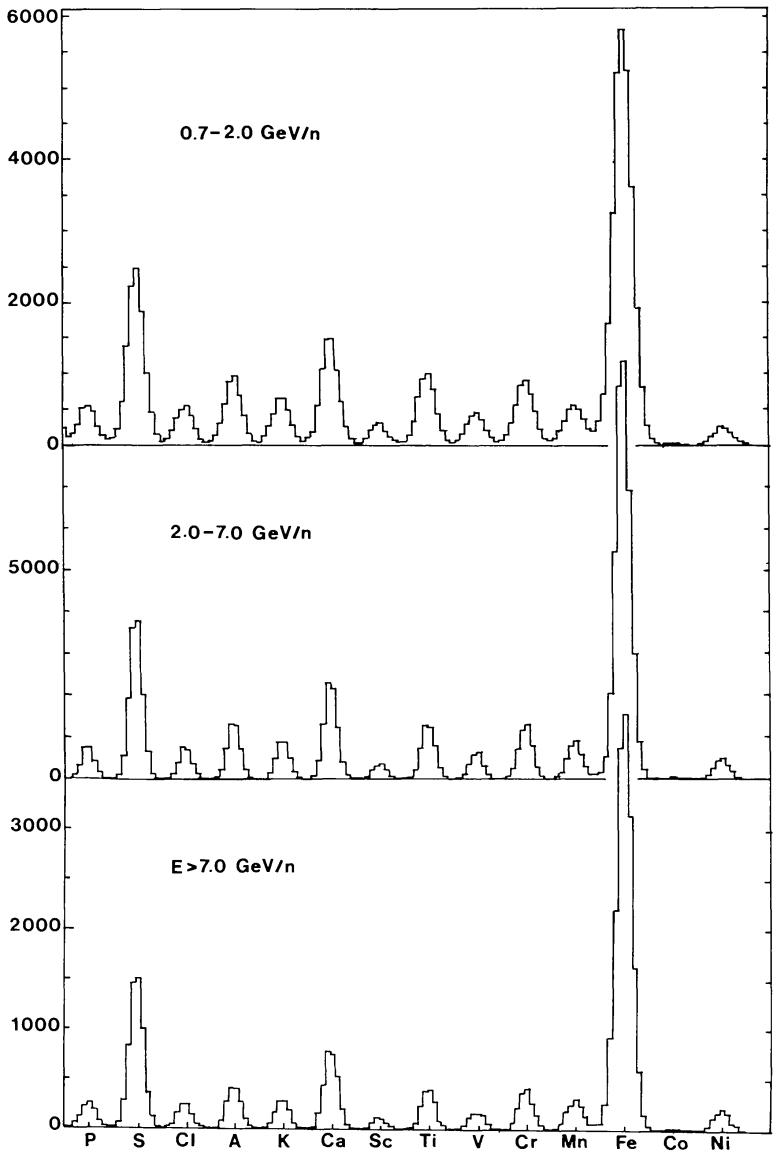

Fig. 17. Charge spectra in three energy ranges.

(4) Scintillation in the Cerenkov radiators.

Analysis of the flight data has shown that the scintillation contribution is only significant in the glass counters (C1 and C5).

In estimating the uncertainty of our momentum assignments we have considered three sources of signal fluctuations:

(1) Poisson fluctuations in the number of photoelectrons liberated in the photomultipliers;

(2) Landau-type fluctuations due to the fluctuations in the number and energy of knock-on electrons contributing to the Cerenkov signal;

(3) Non uniformity of the radiator. This is only important for the aerogel sand

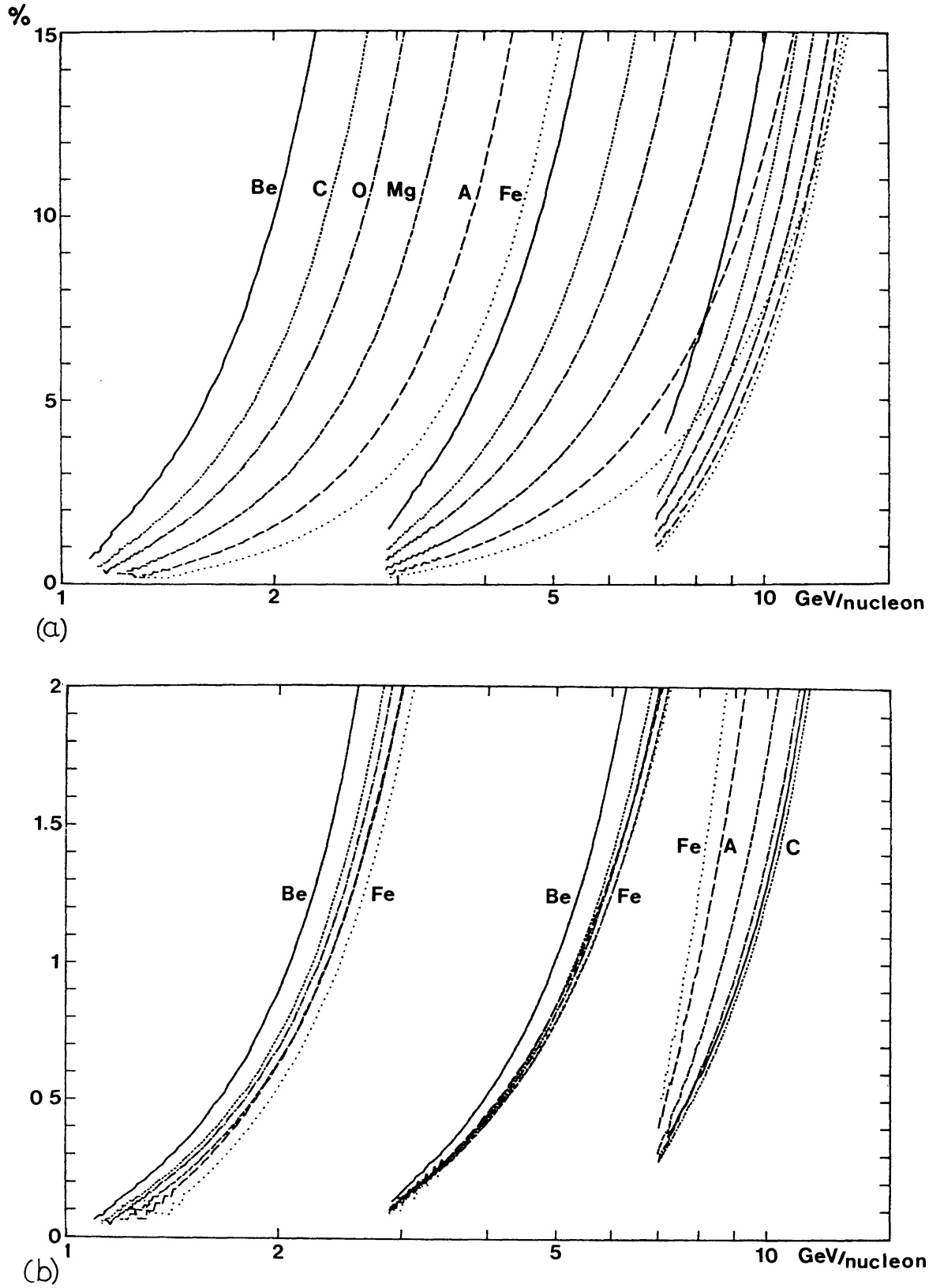

Fig. A1. Momentum resolution in the three velocity counters. (a) Uncertainty in momentum determination. (b) Corresponding uncertainty in mass determination.

counter where the graininess of the radiator leaves an irreducible uncertainty of about 5% in the thickness of radiator material traversed.

Figure A1 illustrates the calculated uncertainty in the momentum determination over the entire momentum range.

Appendix B: Techniques for the Analysis of the Isotopic Composition of Cosmic Rays Using the Geomagnetic Cut-Off

The cosmic rays must have a rigidity higher than the geomagnetic cut-off in order to arrive at a given point inside the geomagnetic field. The value of the cut-off rigidity varies rapidly with particle arrival direction and instrument position inside the field. The inclined orbit of the HEAO-3 satellite therefore requires a wide variety of geomagnetic conditions to be analysed.

We will here group the different methods using the geomagnetic field into integral and differential methods. The schemes used in the integral methods require many particles, but do not demand high precision in the momentum determination or in the knowledge of the magnetic field. The differential methods need fewer particles but higher precision in the momentum and field knowledge to obtain the same information about the mass composition.

INTEGRAL METHODS

The integral methods are based upon the determination of the ratio of the flux of the element under investigation and the flux of a reference element in two different conditions. One ratio, RP, is defined as the ratio of the fluxes above a given momentum/nucleon value P_c, the other ratio, RR, is defined as the ratio of the fluxes above a rigidity R_c which is chosen so as to correspond to P_c for a nucleus with mass $A = 2Z$. The momentum threshold can be selected as a light yield level in the appropriate Cerenkov counter. The two situations can then be realised by using data collected at high magnetic latitudes where the cut-off rigidity is well below R_c to evaluate the RP ratio and data collected at selected latitudes where the cut-off is near R_c to generate the RR ratio.

One can show [2] that the ratio RR/RP depends upon the mean mass of the elements under investigation according to the relations

$$RR = \frac{\sum_i C(Z_1, A_{1i})\left(\frac{Z_1}{A_{1i}}\right)^{\gamma_1}}{\sum_i C(Z_2, A_{2i})\left(\frac{Z_2}{A_{2i}}\right)^{\gamma_2}},$$

$$RP = \frac{\sum_i C(Z_1, A_{1i})}{\sum_i C(Z_2, A_{2i})},$$

$$RR/RP = \frac{\left\langle \left(\frac{Z_1}{A_1}\right)^{\gamma_1} \right\rangle}{\left\langle \left(\frac{Z_2}{A_2}\right)^{\gamma_2} \right\rangle},$$

where gamma is the power law index for the integral flux, $C(Z_i, A_{ij})$ is the relative abundance of the j'th isotope in the i'th element and the sums are taken over all isotopes of the element. This method requires a large number of particles from each element in both of the ratios RR and RP [3]. However the requirements on the precision of the momentum determination and on the knowledge of the effect of the geomagnetic field are minimal.

DIFFERENTIAL METHODS

The differential methods are based upon a close investigation of the momentum spectrum in the penumbra region. For a given position and arrival direction the penumbra is a range of rigidities where forbidden rigidity bands occur above the classical Stoermer cut-off. This is caused by the fact that otherwise allowed trajectories require that the particles passes through the solid Earth prior to their arrival at the instrument position. An estimate of the mean mass can be obtained from a measurement of the shift of the position of the penumbra region between the momentum spectra belonging to different elements. This method is simple to use in a balloon flight where one can observe under roughly constant penumbra conditions for a long time, and it was used in the first determination of isotopic composition at high energies [26]. In a variation of this method one scales the particle momenta according to the Stoermer cut-off in the particle arrival direction, thereby narrowing the region where the transmission factor goes from zero to one [27].

With the C2-instrument it becomes a major part of the data analysis to superimpose data obtained under different penumbra conditions. To be able to quickly identify the penumbra region for any arrival direction and position we have developed interpolation methods based upon a world grid of penumbra patterns [28].

The methods described so far can only determine the mean mass of an element. If the element in question consists of only two isotopes, one can get the relative abundances from the mean mass. In the case of an element with three or more isotopes, one must determine the abundances individually.

We are developing improved methods where we use the observed penumbra transmission function $F(\log(P))$ for oxygen (assumed to be pure O–16) as reference and express the transmission function $G(\log\ (P))$, observed for another element, as a linear combination of isotope contributions each of shape F:

$$G(\log(P)) = \sum_A N_A F\left(\log\left(P\frac{A}{2Z}\right)\right).$$

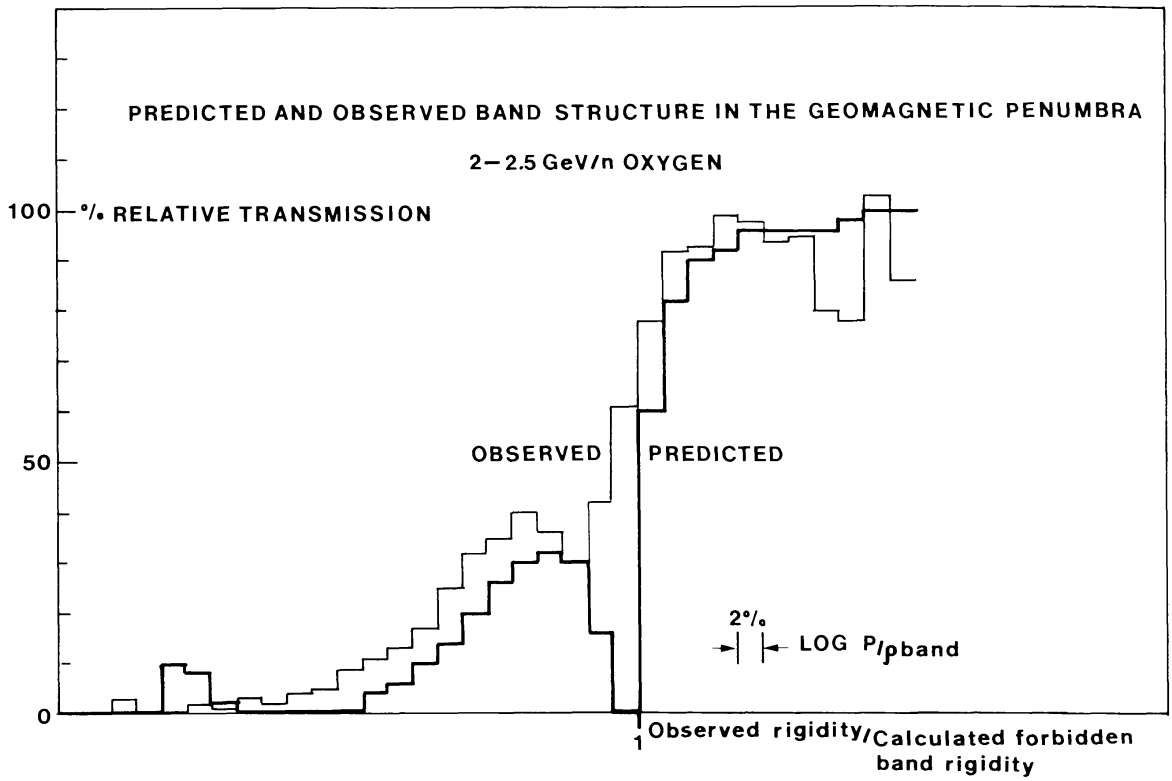

Fig. B1. Plot of rigidity spectrum of oxygen. The rigidity of each particle has been normalized with the calculated value of a persistent penumbra band in the arrival direction. The plot proves the existence of penumbra bands although not at the position predicted by the IGRF–1979 model.

The isotopic abundances N_A can then be determined by a least squares fit. This kind of method is of particular interest in large regions near the magnetic equator where the width of the penumbra is very small (the sharp cut-off region).

At mid and high latitudes, where relatively wide bands of forbidden rigidities can be found in an otherwise allowed rigidity region we try to see a band structure directly in the measured momentum spectra. To be able to follow the rigidity bands over a large geographical area and for different particle arrival directions (to get a large flux), it has been necessary to develop fast trajectory tracing methods so the band position can be calculated for each particle separately. Figure B1 shows the application of this technique to a sample of oxygen particles. It is clear that the position of the forbidden rigidity band shown on the figure is a useful normalization factor although the measured and calculated rigidity value differs by several percent.

References

[1] Lund, N., Peters, B., Cowsik, R., and Pal, Y.: 1970, *Phys. Lett.* **31B**, 553.
[2] Lund, N., Rasmussen, I. L., and Peters, B.: 1971, *12th International Cosmic Ray Conference*, Vol. **1**, p. 130.
[3] Peters, B.: 1974, *Nucl. Instrum. Meth.* **121**, 205.

[4] Petrou, N. and Soutoul, A.: 1977, *15th International Cosmic Ray Conference*, Vol. **11**, p. 273.
[5] Byrnak, B., Lund, N., and Sorgen, A.: 1979, in W. Riedler (ed.), *Scientific Ballooning*, Pergamon, p. 155.
[6] Arnett, W. D. and Schramm, D. N.: 1973, *Astrophys. J. Letters* **184**, L47.
[7] Hainebach, K. L., Norman, E. B., and Schramm, D. N.: 1976, *Astrophys. J.* **203**, 245.
[8] Soutoul, A., Casse, M., and Juliusson, E.: 1978, *Astrophys. J.* **219**, 753.
[9] Casse, M. and Goret, P.: 1973, *13th International Cosmic Ray Conference*, Vol. **1**, p. 584.
[10] Eichler, D.: 1980, *Astrophys. J.* **237**, 809.
[11] Fransson, C. and Epstein, R.: 1980, *Astrophys. J.* **242**, 411.
[12] Heckman, H. H., Greiner, D. E., Lindstrom, P. J., and Bieser, F. S.: 1972, *Phys. Rev. Letters* **28**, 926.
[13] Lindstrom, P. J., Greiner D. E., Heckman, H. H., Cork, B., and Bieser, F. S.: 1975, LBL Report 3650.
[14] Westfall, G. D., Wilson, L. W., Lindstrom, P. J., Crawford, H. J., and Heckman, H. H.: 1979, *Phys. Rev.* **C19**, 1309.
[15] Lund, N., Rasmussen, I. L., Peters, B., and Westergaard, N. J.: 1975, *14th International Cosmic Ray Conference*, Vol. **1**, p. 2527.
[16] Rasmussen, I. L. and Peters, B.: 1975, *Nature* **258**, 412.
[17] Corydon-Petersen, O., Dayton, B., Lund, N., Melgaard, K., Omoe, K., Peters, B., and Risbo, T.: 1970, *Nucl. Instrum. Meth.* **81**, 1.
[18] Cantin, M., Goret, P., Jorrand, J., Jouan, R., Juliusson, E., Koch, L., Maubras, Y., Mestreau, P., Petrou, N., Rio, Y., Soutoul, A., Cawood, P., and Linney, A.: 1975, *14th International Cosmic Ray Conference*, Vol. **9**, p. 3211.
[19] Linney, A. and Peters, B.: 1972, *Nucl. Instrum. Meth.* **100**, 545.
[20] Koch, L.: 1973, *Bull. Inf. Sci. Tech.* **187**, 3.
[21] Cantin, M., Casse, M., Koch, L., Jouan, R., Mestreau, P., and Roussel, D.: 1974, *Nucl. Instrum. Meth.* **118**, 177.
[22] Goret, P. and Evenson, P.: Private communication.
[23] Engelmann, J. J. and Cantin, M.: 1978, *J. Phys.* **39**, C3–57.
[24] Andrews, D., Corydon-Petersen, O., Funch, O., and Rotenberg, M.: 1971, *12th International Cosmic Ray Conference*, Vol. **4**, p. 1543.
[25] Funch, O. Iversen, I. B., Lund, N., Rasmussen, I. L., and Rotenberg, M.: 1973, *13th International Cosmic Ray Conference*, Vol. **4**, p. 3023.
[26] Dwyer R. and Meyer, P.: 1975, *Phys. Rev. Letters* **35**, 601.
[27] Hubert, P.: 1974, *Nucl. Instrum. Meth.* **119**, 183.
[28] Smart, D. F., Shea, M. A., Lund, N., Rasmussen, I. L., Byrnak, B., and Westergaard, N. J.: 1979, *16th International Cosmic Ray Conference*, Vol. **12**, p. 237.